RAPID COMMUNICATIONS

PHYSICAL REVIEW B **96**, 081408(R) (2017)

# Effects of optical polarization on hybridization of radiative and evanescent field modes

Andrii Iurov,[1] Danhong Huang,[2] Godfrey Gumbs,[3] Wei Pan,[4] and A. A. Maradudin[5]
[1]*Center for High Technology Materials, University of New Mexico, 1313 Goddard SE, Albuquerque, New Mexico 87106, USA*
[2]*Air Force Research Laboratory, Space Vehicles Directorate, Kirtland Air Force Base, New Mexico 87117, USA*
[3]*Department of Physics and Astronomy, Hunter College of the City University of New York, 695 Park Avenue, New York, New York 10065, USA*
[4]*Sandia National Laboratories, Albuquerque, New Mexico 87185, USA*
[5]*Department of Physics and Astronomy, University of California, Irvine, California 92697, USA*
(Received 12 June 2017; published 23 August 2017)

The effects of induced optical polarization by Dirac electrons in graphene on the hybridization of radiative and evanescent fields are found. Such effects result in a localized polarization field which significantly modifies an incident surface-plasmon-polariton (SPP) field. This yields a high sensitivity to local dielectric environments and provides an investigative tool for molecules or proteins selectively bound with carbons. A scattering matrix is utilized with varied frequencies in the vicinity of the surface-plasmon (SP) resonance for the increase, decrease, and even a full suppression of the polarization field, which enables accurate effective-medium theories to be constructed for Maxwell-equation finite-difference time-domain methods. Moreover, double peaks in the absorption spectra for hybrid SP and graphene-plasmon modes are significant only with a large conductor plasma frequency, but are overshadowed by a round SPP peak at a small plasma frequency as the graphene is placed close to the conductor surface. These resonant absorptions facilitate polariton-only excitations, leading to polariton condensation for a threshold-free laser.

DOI: 10.1103/PhysRevB.96.081408

*Introduction*. It is known that when light is incident on a semiconductor, its energetic photons can elevate electrons from a valence band to a conduction band, leaving many electron-hole pairs in the system [1,2]. Simultaneously, its electric-field component will further move aside these negatively (positively) charged electrons (holes) in opposite spatial directions. However, the remaining question is, *do excited electrons or the holes exert an action back on the incident light?* The answer to this lies in the induced optical-polarization field as a collection of local dipole moments from many displaced electrons and holes [3,4], which plays a role in scattering the electric-field component of the incident light [5,6]. Therefore, the quantum nature of Dirac electrons [7–11] is expected to be retained in the effects of optical polarization on the incident light with a complex distribution of the Landau-damping regions in comparison with that for two-dimensional electron gases in a quantum well [12].

For a hybrid structure illustrated in Fig. 1(a), we encounter radiative field modes, such as photons and polaritons [13–17], as well as evanescent field modes, e.g., surface and graphene plasmons [18–20]. Research on the optical responses of graphene electrons has been reported previously [20,21], but most of those efforts have been limited to the radiation or grating-deflection field coupling. In contrast to a plane-wave-like external field, we explore surface-plasmon-polariton near-field [22–24] coupling to graphene electrons with a different dispersion relation from the usual linear one, i.e., $\omega = qc$, for free-space light. In our case, graphene is brought very close to the surface of a conducting substrate so that the hybridization of radiative and evanescent fields can occur [25]. Consequently, the non-dispersive surface-plasmon mode is able to hybridize with radiative photon and polariton modes [13,14], as well as with the spatially localized graphene plasmon mode [12], as shown schematically in Fig. 1(b).

Such a distinctive dispersion relation of hybrid quantum-plasmon modes should be experimentally observable in optical spectra [26–29]. The effective scattering matrix [30,31] from such a coupled system is found to differ significantly from that for either graphene or the conductor and it displays distinctive features from the retarded longitudinal Coulomb interaction [6] between electrons in graphene and the conductor. This scattering matrix can be employed for constructing an effective-medium theory [9,32–35] and investigating the optical properties of inserted biomolecules and metamaterials between the graphene sheets and the surface of the conductor. Therefore, locally environment-sensitive super-resolution near-field imaging can be developed for functionalized biomolecules bound to metallic nanodots and nanorods or even carbon atoms of graphene [36].

*Theory and methods*. The structure under investigation is illustrated in Fig. 1(a), and consists of a thick conductor and a dielectric-embedded graphene above its surface. A surface-plasmon-polariton field (SPPF) can be excited by incident light on a surface grating. This surface-propagating SPPF couples to Dirac electrons in graphene, and the induced polarization field from graphene acts back simultaneously on the SPPF as a resonant scatterer. Details about the derivations of Eqs. (1)–(4) below can be found in Ref. [37].

Using the Green's function approach [5], we convert Maxwell's equation for the electric field $\boldsymbol{E}(\mathbf{r},\omega)$ into an integral equation in the spatial ($\mathbf{r}$) domain, including a nonlocal source term to scatter the incident SPPF $\boldsymbol{\mathcal{E}}^{\rm inc}(\mathbf{r},\omega)$, where $\omega$ is the light frequency. After Fourier transforming this integral equation with respect to $\mathbf{r}_\parallel$, we obtain ($\mu,\nu = 1,2,3$)

$$E_\mu(\mathbf{q}_\parallel,\omega|x_3) = \mathcal{E}^{\rm inc}_\mu(\mathbf{q}_\parallel,\omega|x_3) + \frac{\omega^2}{\epsilon_0 c^2}\sum_\nu g_{\mu\nu}(\mathbf{q}_\parallel,\omega|x_3,z_0)\mathcal{P}^{\rm s}_\nu(\mathbf{q}_\parallel,\omega), \qquad (1)$$

where $\mathbf{r} = \{\mathbf{r}_\parallel,x_3\}$, $x_3 = z_0$ denotes the graphene-sheet position, and $g_{\mu\nu}(\mathbf{q}_\parallel,\omega|x_3,z_0)$ is the Fourier transformed Green's function matrix [6] which corresponds to a retarded coupling

2469-9950/2017/96(8)/081408(5)

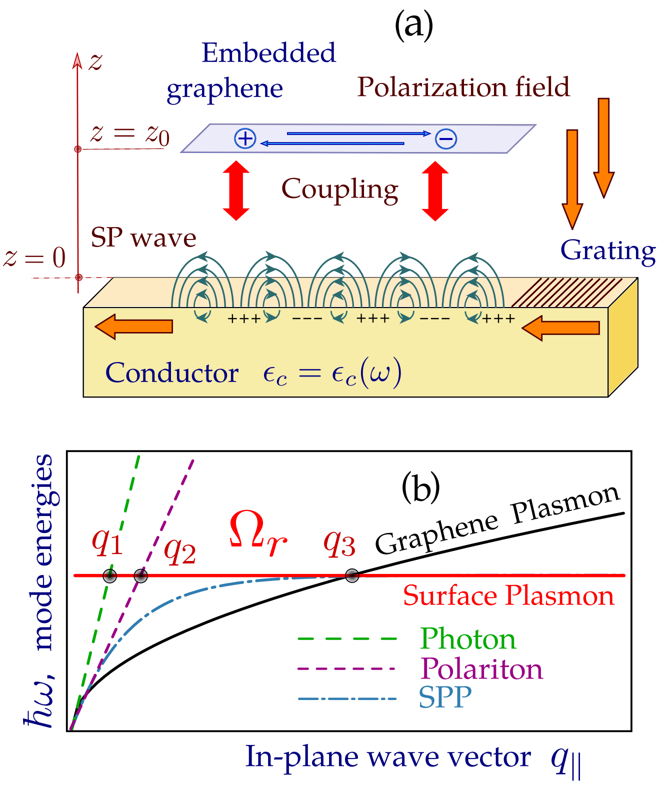

FIG. 1. (a) Schematic for a thick conductor ($z < 0$) with dielectric function $\epsilon_c(\omega)$ and a graphene layer at $z = z_0$ above its surface at $z = 0$ which is embedded within a semi-infinite material, extending from $z = 0$ to $z = \infty$, with dielectric constant $\epsilon_d$. The surface-plasmon-polariton field (SPPF) is excited by light incident on a grating. The propagating SPPF excites Dirac electrons in graphene and induced graphene polarization modifies the SPPF by resonant scattering. (b) Illustration for energy dispersion of photons, polaritons, surface-plasmon polaritons (SPPs), graphene plasmons (GPs), and surface plasmons (SPs), where the three labeled circles indicate the mode hybridizations.

between graphene electrons to the incident SPPF. Using linear response theory [38], we obtain the graphene polarization field in Eq. (1), $\mathcal{P}^{\rm s}_\nu(\mathbf{q}_\parallel,\omega) = \epsilon_0\chi^{(0)}_{\rm s}(q_\parallel,\omega)(1-\delta_{\nu3})E_\nu(\mathbf{q}_\parallel,\omega|z_0)$, where $\chi^{(0)}_{\rm s}(q_\parallel,\omega) = e^2\,\Pi^{(0)}_{\rm s}(q_\parallel,\omega)/[\epsilon_0(q^2_\parallel - \epsilon_{\rm d}\,\omega^2/c^2)]$ [39], and $\Pi^{(0)}_{\rm s}(q_\parallel,\omega)$ is the density-density correlation function for graphene electrons [40–42]. The transverse and longitudinal electronic responses are associated with the magnetic and electric susceptibilities, respectively. The former is usually much weaker than the latter if no magnetic impurities are present in the graphene layer. In this Rapid Communication, we will concentrate on the dominant scattering of the incident SPP electric field from the dielectric response of graphene while simultaneously neglecting the graphene diamagnetic response The properties of the graphene diamagnetic response have been discussed before by using the lattice model [43,44]. Setting $x_3 = z_0$ in Eq. (1), we obtain a self-consistent equation for $\boldsymbol{E}(\mathbf{q}_\parallel,\omega|z_0)$. Furthermore, if $\boldsymbol{\mathcal{E}}^{\rm inc}(\mathbf{q}_\parallel,\omega|z_0) = 0$ is assumed in this self-consistent equation, we obtain the dispersion equation for the hybrid-plasmon modes, and the resulting dispersion relation $\omega = \Omega(\mathbf{q}_\parallel|z_0)$, as illustrated in Fig. 1(b), is determined from the real part of the secular equation $\mathrm{Det}\{\overleftrightarrow{\mathcal{C}}(\mathbf{q}_\parallel,\omega|z_0)\} = 0$, where $\overleftrightarrow{\mathcal{C}}(\mathbf{q}_\parallel,\omega|z_0) = \delta_{\mu\nu} - (\omega/c)^2 g_{\mu\nu}(\mathbf{q}_\parallel,\omega|z_0,z_0)(1-\delta_{\nu3})\chi^{(0)}_{\rm s}(q_\parallel,\omega)$ is the complex coefficient matrix. After calculating the inverse of $\overleftrightarrow{\mathcal{C}}$, $\boldsymbol{E}(\mathbf{r}_\parallel,\omega|x_3)$ can be expressed explicitly as

$$E_\mu(\mathbf{r}_\parallel,\omega|x_3) = \mathcal{E}^{\rm inc}_\mu(\mathbf{r}_\parallel,\omega|x_3) + \frac{\omega^2}{c^2}\int\frac{d^2\mathbf{q}_\parallel}{(2\pi)^2}\,e^{i\mathbf{q}_\parallel\cdot\mathbf{r}_\parallel}\,\chi^{(0)}_{\rm s}(q_\parallel,\omega)$$
$$\times\sum_\nu\Bigg\{g_{\mu\nu}(\mathbf{q}_\parallel,\omega|x_3,z_0)(1-\delta_{\nu3})$$
$$\times\Bigg[\sum_{\mu'}\mathcal{C}^{-1}_{\nu\mu'}(\mathbf{q}_\parallel,\omega|z_0)\mathcal{E}^{\rm inc}_{\mu'}(\mathbf{q}_\parallel,\omega|z_0)\Bigg]\Bigg\}. \qquad (2)$$

From Eq. (2), the Fourier transformed scattering matrix [30] is readily determined to be given as

$$\alpha^{\rm eff}_{\mu\nu}(\mathbf{q}_\parallel,\omega|x_3) = \frac{\omega^2}{c^2}\,\chi^{(0)}_{\rm s}(q_\parallel,\omega)\sum_{\nu'}g_{\mu\nu'}(\mathbf{q}_\parallel,\omega|x_3,z_0)$$
$$\times(1-\delta_{\nu'3})\mathcal{C}^{-1}_{\nu'\nu}(\mathbf{q}_\parallel,\omega|z_0). \qquad (3)$$

Additionally, by using the calculated $\boldsymbol{E}(\mathbf{r}_\parallel,\omega|z_0)$ in Eq. (2), the absorption coefficient $\beta_{\rm abs}(\omega|z_0)$ for the SPPF can be calculated [22,45] based on the Lorentz function $\alpha_{\rm L}(\omega|z_0)$ given by

$$\alpha_{\rm L}(\omega|z_0) = \frac{c}{\omega}\Bigg|\sum_{\mu,\nu}\hat{e}_\mu\,\mathcal{C}^{-1}_{\mu\nu}(\boldsymbol{k}_0,\omega|z_0)[i\hat{k}_\nu\beta_3(\omega) - \hat{x}_\nu k_0(\omega)]$$
$$\times e^{-\beta_3(\omega)z_0}\Bigg|\left(\frac{2\pi e^2}{\epsilon_0\epsilon_{\rm r}k_0}\right)\sqrt{1-\frac{\epsilon_{\rm d}\omega^2}{k_0^2c^2}}\{\Pi^{(0)}_{\rm s}(k_0,\omega)$$
$$+\left[\Pi^{(0)}_{\rm s}(k_0,-\omega)\right]^*\}, \qquad (4)$$

where $\epsilon_{\rm r}$ is the effective dielectric constant of the host material above the conductor surface in which the graphene layer is embedded and is approximately taken as the cladding-layer dielectric constant $\epsilon_{\rm d}$, $\hat{\boldsymbol{e}}$ and $\hat{\boldsymbol{k}}$ are the unit polarization and wave vectors of the SPPF, $\hat{\boldsymbol{x}} = (0,0,1)$ is the spatial unit vector, $\boldsymbol{k}_0 \equiv \mathrm{Re}[k_0(\omega)]\hat{\boldsymbol{k}}$, $\beta_3(\omega) = \sqrt{k_0^2(\omega) - \omega^2/c^2}$, $k_0(\omega) = (\omega/c)\sqrt{\epsilon_{\rm d}\epsilon_{\rm c}(\omega)/[\epsilon_{\rm d}+\epsilon_{\rm c}(\omega)]}$, $\epsilon_{\rm d}$ is the cladding-layer dielectric constant, $\epsilon_{\rm c}(\omega) = \epsilon_{\rm s} - \Omega_p^2/[\omega(\omega + i0^+)]$ for the conductor, and $\mathrm{Re}[k_0(\omega)] \geqslant 0$ as well as $\mathrm{Re}[\beta_3(\omega)] \geqslant 0$ are assumed in treating the multivalue square roots [37].

*Results and discussions*. In our numerical calculations, we use the Fermi wave vector $k_{\rm F} = \sqrt{\pi n_0}$ as the scale for wave numbers, $1/k_{\rm F}$ for lengths, and $E_{\rm F} = \hbar v_{\rm F}k_{\rm F}$ for energies. The direction of SPPF propagation is chosen as $\hat{\boldsymbol{k}} = (1,0,0)$ for simplicity, and we also set $\epsilon_{\rm s} = 13.3$, $\epsilon_{\rm d} = \epsilon_{\rm r} = 2.4$, $v_{\rm F} = 1\times10^8$ cm/s, and $n_0 = 5\times10^{11}$ cm$^{-2}$ for the doping density in graphene. Moreover, the half gap $\Delta = 0$ is assumed unless it is stated in figure captions, and the resonant frequency $\Omega_r = \Omega_p/\sqrt{\epsilon_{\rm s}+\epsilon_{\rm d}}$ will be given directly in the figure captions.

For a retarded interaction between light and graphene electrons, both radiative and evanescent modes must be considered for the hybrid structure. The radiative modes include photons and polaritons, while the evanescent modes appear as surface-plasmon polaritons (SPPs), graphene plasmons (GPs), and surface plasmons (SPs). Figure 2 presents the real part of

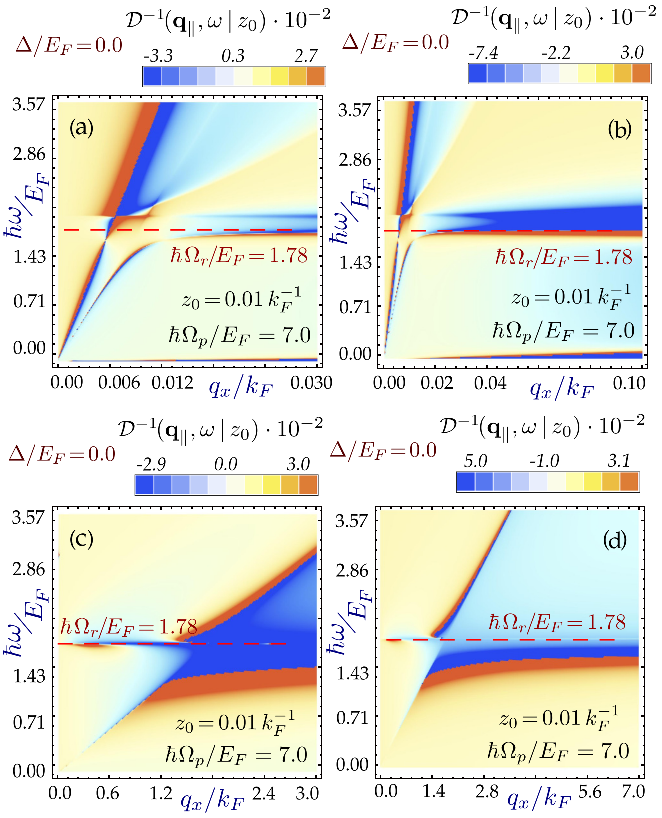

FIG. 2. Density plots for the real part of $\mathcal{D}^{-1}(q_x,\omega|z_0) \equiv 1/\mathrm{Det}\{\overleftrightarrow{\mathcal{C}}(q_x,\omega|z_0)\}$ in four different $q_x$ ranges growing from 0.03 to 7 with hybrid-plasmon dispersions indicated by jumps between positive (red) and negative (blue) peaks. Here, $k_F z_0 = 0.01$, $\hbar\Omega_r/E_F = 1.78$.

$\mathcal{D}^{-1}(q_x,\omega|z_0) \equiv 1/\mathrm{Det}[\overleftrightarrow{\mathcal{C}}(q_x,\omega|z_0)]$ for four chosen $q_x$ ranges. It is clear from Fig. 2(a) that in addition to the SPP mode, the hybridizations of both radiative photon and polariton modes with localized SPs [labeled as $q_1$ and $q_2$ in Fig. 1(b)] appear in this very small $q_x$ range. As the $q_x$ range is slightly expanded in Fig. 2(b), the SPP mode in Fig. 2(a) becomes fully developed, which is accompanied by a GP mode at low energies. As the $q_x$ range is further increased in Figs. 2(c) and 2(d), the GP energy exceeds that of the SP. Consequently, the anticrossing of GPs with SPPs [labeled by $q_3$ in Fig. 1(b)] is observed.

The $z_0$ dependence in the secular equation highlights the nature of the distinctive evanescent coupling between SPPs and GPs. Here, the factor $g_{\mu\nu}(q_x,\omega|z_0,z_0)$ plays the role of a retarded SPP coupling to a spatially separated GP, while $\chi_s^{(0)}(q_x,\omega)$ corresponds to the GP optical response. Therefore, their product represents the hybrid Dirac-SPP modes. By moving the graphene a bit further from the conductor surface, the anticrossing gap shrinks due to decreased retarded coupling. Simultaneously, the strengths of all the plasmon, polariton, and photon modes increase by more than one order of magnitude due to loss suppression of these modes to the conductor.

The incident SPPF suffers not only Ohmic loss during its propagation along the conductor surface, but also absorption loss by its coupling to GPs. Figure 3 presents the absorption spectra $\beta_{\mathrm{abs}}(\omega|z_0)$ for various $\Delta$ in Fig. 3(a) and chosen $z_0$ in Fig. 3(b). From Fig. 3(a) we find three absorption peaks for $\Delta = 0$, where two sharp ones correspond to GPs (right) and SPs (left), as seen from Figs. 2(c) and 2(d), with a deep trough separating them for the opened anticrossing gap labeled as $q_3$ in Fig. 1(b). The lowest rounded peak is for SPP modes, as shown in Figs. 2(a) and 2(b), which is separated from the SP peak by a shallow dip labeled by $q_2$ in Fig. 1(b). The absorption peak from the indistinguishable SPP and SP modes increases greatly in the inset of Fig. 3(a) for a lower SP resonance $\hbar\Omega_r/E_F = 0.25$ since the SPPF decay is largely eased at a much smaller $q_x$. The enhancement of the SPP absorption peak is also observed in Fig. 3(b) for small $z_0$ due to reduced SPPF decay. Moreover, we find from the inset of Fig. 3(b) that the decrease of $\beta_{\mathrm{abs}}(\omega|z_0)$ with increasing $z_0$ becomes much more dramatic as $\omega$ approaches $\Omega_r$ with increased SPPF localization.

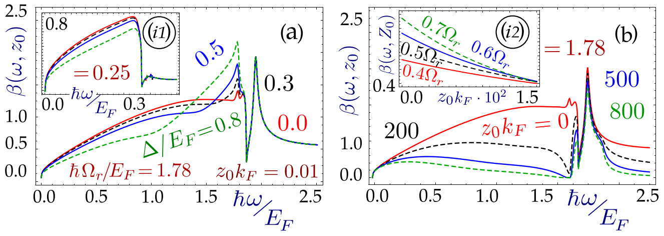

FIG. 3. Absorption spectra $\beta_{\mathrm{abs}}(\omega|z_0)$ [in units of $k_F$] displayed in (a) with $k_F z_0 = 0.01$ for $\Delta/E_F = 0, 0.1, 0.3, 0.8$, where $\hbar\Omega_r/E_F = 1.78$ and 0.25 in its inset. In (b), $\beta_{\mathrm{abs}}(\omega|z_0)$ with $\hbar\Omega_r/E_F = 1.78$, $\Delta/E_F = 0$ for $k_F z_0 = 0, 200, 500, 800$, and its $z_0$ dependence in the inset for $\omega/\Omega_r = 0.4, 0.5, 0.6, 0.7$.

In addition to the SPPF optical absorption by GPs, resonant scattering of the SPPF from GPs also takes place, as described by Eq. (3). Figure 4 presents three-dimensional (3D) plots for $[\mathrm{Re}\{\alpha_{11}^{\mathrm{eff}}(q_x,\omega|x_3)\}]^{1/5}$ with four values for $\omega$, where the graphene is positioned relatively close to the surface. Here,

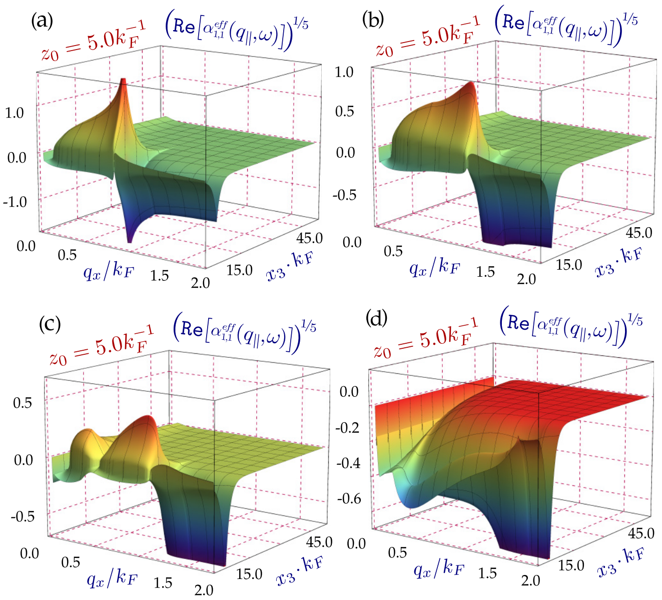

FIG. 4. 3D plots for $[\mathrm{Re}\{\alpha_{11}^{\mathrm{eff}}(q_x,\omega|x_3)\}]^{1/5}$ with (a) $\omega/\Omega_r = 0.7$, (b) 0.8, (c) 0.9, (d) 1.0, where $k_F z_0 = 5$, $\hbar\Omega_r/E_F = 1.78$.

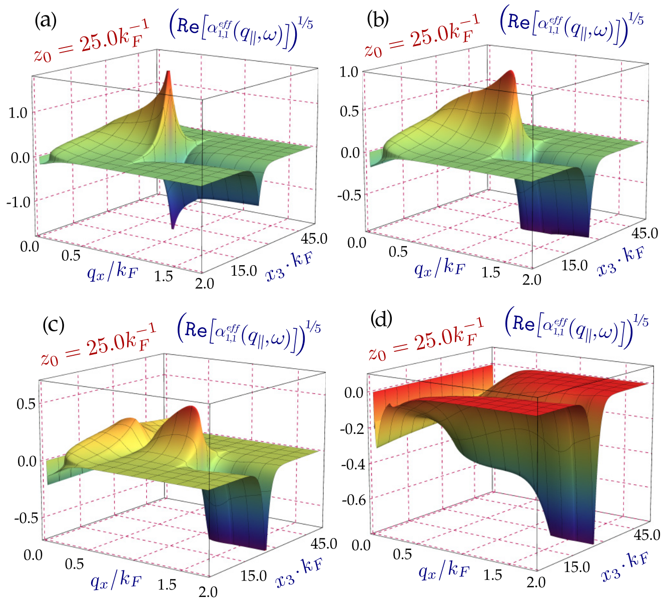

FIG. 5. 3D plots for $[\mathrm{Re}\{\alpha_{11}^{\mathrm{eff}}(q_x,\omega|x_3)\}]^{1/5}$ with (a) $\omega/\Omega_r = 0.7$, (b) 0.8, (c) 0.9, (d) 1.0, where $k_{\mathrm{F}} z_0 = 25$, $\hbar\Omega_r/E_{\mathrm{F}} = 1.78$.

the scattering matrix is $\alpha_{\mu\nu}^{\mathrm{eff}} \equiv \delta(E_\mu - \mathcal{E}_\mu^{\mathrm{inc}})/\delta\mathcal{E}_\nu^{\mathrm{inc}}$, and its signs correspond to enhanced (+) or weakened (−) SPPF after light scattering with GPs. The left (right) and lower (upper) regions correspond to small (large) $q_x$ and $x_3$, respectively. If both $q_x$ and $x_3$ are large, such scattering is significantly suppressed, leaving only a sizable and flat basin in the upper-right-hand corners of Figs. 4(a)–4(d). If $q_x$ is very small, the photon and SPP radiative modes dominate, and then $\mathrm{Re}\{\alpha_{11}^{\mathrm{eff}}(q_x,\omega|x_3)\}$ remains negative and becomes independent of $x_3$. When $q_x$ is intermediate, the SPP evanescent modes start entering in with increasing $\omega$ up to $\Omega_r$. In this case, the positive peak strength is reduced and the peak coverage is squeezed into a smaller $x_3$ region where the localization of SPPF is still insignificant. Even more, the positive peak is split into two islands at $\omega = 0.9\Omega_r$ and it is eventually switched to a negative peak followed by a negative edge at $\omega = \Omega_r$. On the other hand, when $q_x$ becomes very large for a strongly localized SPPF, its scattering by GP becomes negligible except for the region very close to the graphene, as shown by the sharp negative edges in the lower-right-hand corners of Figs. 4(a)–4(d).

By moving the graphene further away from the conductor surface, as shown in Fig. 5, we expect the scattering effects from GPs on the SPPF to be limited to a narrow area surrounding the graphene for large $q_x$ values. Indeed, when $q_x$ is large, we find $\mathrm{Re}\{\alpha_{11}^{\mathrm{eff}}(q_x,\omega|x_3)\} = 0$ for $x_3$ far away from the graphene at $z_0$ in the upper- and lower-right-hand corners of Figs. 5(a)–5(d). For small $q_x$ values, however, the positive peak appears, as in Fig. 5, and its coverage crawls out along $x_3 = z_0$ to a relative large $q_x$ region, followed by a negative sharp edge, although its peak strength decreases with increasing $\omega$ towards $\Omega_r$. This extended region becomes separated from the positive peak at $\omega = 0.9\Omega_r$ in Fig. 5(c) to form an island, and both the positive peak and island disappear and are eventually replaced by negative sharp and stepped edges at $\omega = \Omega_r$ in Fig. 5(d).

*Summary*. The effect of induced optical polarization on the hybridization of radiative and evanescent fields has been demonstrated by using a retarded interaction, which is seen as the hybrid dispersions for both radiative (small $q_x$ range) and evanescent (large $q_x$ range) field modes. Such an effect is rooted in the induced optical-polarization field from the Dirac plasmons, which resonantly redistributes an incident surface-plasmon-polariton field by scattering. The localization characteristics of such a retarded interaction ensure high sensitivity to dielectric environments surrounding graphene, including variations in the conducting substrate, cladding layer, electronic properties of embedded graphene, as well as the graphene distance from the conductor surface. This provides a unique advantage in wavelength-sensitive optical investigation of chemically active molecules or proteins bound to carbon atoms in graphene [5,6].

The optical probing tools discussed in this Rapid Communication include either scattering or optical absorption of an incident electromagnetic field. For light scattering, we calculated the spatial-temporal dependence of a Fourier transformed scattering matrix, which clearly exhibits the scattering enhancement, weakening, and even suppression as functions of both graphene separations ($z_0$) from the conductor surface and wave numbers ($q_x$) of the evanescent surface-plasmon-polariton field at several frequencies close to the localized surface-plasmon resonance. This derived scattering matrix lays the foundation for constructing an effective-medium theory commonly employed in finite-difference time-domain methods [46] for solving Maxwell's equations. For field absorption, the double peaks associated with hybrid surface and graphene plasmon modes on the high-energy side are shown to be dominant for high conductor plasma frequencies and small graphene separations. However, the rounded peak on the low-energy side plays the dominant role at low plasma frequencies. Additionally, this rounded peak shows that SPP modes can be greatly enhanced when graphene is moved close to the surface of the conductor. These unique features in resonant absorption enable the selective excitation of radiative polariton modes for their condensation and a threshold-free laser afterwards.

*Acknowledgment.* D.H. is thankful for support from the Air Force Office of Scientific Research (AFOSR).

---

[1] H. Haug and S. W. Koch, *Quantum Theory of the Optical and Electronic Properties of Semiconductors*, 4th ed. (World Scientific Publishing, Singapore, 2004).
[2] F. Rossi and T. Kuhn, Rev. Mod. Phys. **74**, 895 (2002).
[3] M. Lindberg and S. W. Koch, Phys. Rev. B **38**, 3342 (1988).
[4] M. Kira and S. W. Koch, Prog. Quantum Electron. **30**, 155 (2006).
[5] D. H. Huang, M. M. Easter, G. Gumbs, A. A. Maradudin, S.-Y. Lin, D. A. Cardimona, and X. Zhang, Opt. Express **22**, 27576 (2014).

[6] D. H. Huang, M. M. Easter, G. Gumbs, A. A. Maradudin, S.-Y. Lin, D. A. Cardimona, and X. Zhang, Appl. Phys. Lett. **104**, 251103 (2014).

[7] K. Novoselov, A. K. Geim, S. Morozov, D. Jiang, M. Katsnelson, I. Grigorieva, S. Dubonos, and A. Firsov, Nature (London) **438**, 197 (2005).

[8] A. K. Geim and K. S. Novoselov, Nat. Mater. **6**, 183 (2007).

[9] K. K. Gomes, W. Mar, W. Ko, F. Guinea, and H. C. Manoharan, Nature (London) **483**, 306 (2012).

[10] Y. Zhang, Y.-W. Tan, H. L. Störmer, and P. Kim, Nature (London) **438**, 201 (2005).

[11] A. K. Geim, Science **324**, 1530 (2009).

[12] A. Iurov, G. Gumbs, D. Huang, and V. M. Silkin, Phys. Rev. B **93**, 035404 (2016).

[13] S. Christopoulos, G. Baldassarri Höger von Högersthal, A. J. D. Grundy, P. G. Lagoudakis, A. V. Kavokin, J. J. Baumberg, G. Christmann, R. Butté, E. Feltin, J.-F. Carlin, and N. Grandjean, Phys. Rev. Lett. **98**, 126405 (2007).

[14] S. I. Tsintzos, N. T. Pelekanos, G. Konstantinidis, Z. Hatzopoulos, and P. G. Savvidis, Nature (London) **453**, 372 (2008).

[15] P. Bhattacharya, B. Xiao, A. Das, S. Bhowmick, and J. Heo, Phys. Rev. Lett. **110**, 206403 (2013).

[16] C. Schneider, A. Rahimi-Iman, N. Y. Kim, J. Fischer, I. G. Savenko, M. Amthor, M. Lermer, A. Wolf, L. Worschech, V. D. Kulakovskii, I. A. Shelykh, M. Kamp, S. Reitzenstein, A. Forchel, Y. Yamamoto, and S. Höfling, Nature (London) **497**, 348 (2013).

[17] E. L. Albuquerque and M. G. Cottam, Phys. Rep. **233**, 67 (1993).

[18] B. Wang, X. Zhang, F. J. García-Vidal, X. Yuan, and J. Teng, Phys. Rev. Lett. **109**, 073901 (2012).

[19] M. Liu, X. Yin, and X. Zhang, Nano Lett. **12**, 1482 (2012).

[20] M. Liu, X. Yin, E. Ulin-Avila, B. Geng, T. Zentgraf, L. Ju, F. Wang, and X. Zhang, Nature (London) **474**, 64 (2011).

[21] F. Koppens, T. Mueller, P. Avouris, A. Ferrari, M. Vitiello, and M. Polini, Nat. Nanotechnol. **9**, 780 (2014).

[22] A. A. Maradudin and D. L. Mills, Phys. Rev. B **11**, 1392 (1975).

[23] M. G. Cottam and A. A. Maradudin, in *Surface Excitations*, edited by V. M. Agranovich and R. Loudon (North-Holland, Amsterdam, 1984), pp. 1–194.

[24] J. M. Pitarke, V. M. Silkin, E. V. Chulkov, and P. M. Echenique, Rep. Prog. Phys. **70**, 1 (2007).

[25] A. V. Zayats, I. I. Smolyaninov, and A. A. Maradudin, Phys. Rep. **408**, 131 (2005).

[26] M. S. Tame, K. R. McEnery, S. K. Özdemir, J. Lee, S. A. Maier, and M. S. Kim, Nat. Phys. **9**, 329 (2013).

[27] F. de León-Pérez, G. Brucoli, F. J. García-Vidal, and L. Martín-Moreno, New J. Phys. **10**, 105017 (2008).

[28] A. N. Grigorenko, M. Polini, and K. S. Novoselov, Nat. Photon. **6**, 749 (2012).

[29] D. N. Basov, M. M. Fogler, A. Lanzara, F. Wang, and Y. Zhang, Rev. Mod. Phys. **86**, 959 (2014).

[30] D. S. Saxon, Phys. Rev. **100**, 1771 (1955).

[31] F. J. García de Abajo, Rev. Mod. Phys. **79**, 1267 (2007).

[32] J. van Kranendonk and J. E. Sipe, in *Progress in Optics XV*, edited by E. Wolf (North-Holland, New York, 1977), Chap. 5.

[33] G. D. Mahan and G. Obermair, Phys. Rev. **183**, 834 (1969).

[34] J. Sipe and J. van Kranendonk, Phys. Rev. A **9**, 1806 (1974).

[35] W. Lamb, D. M. Wood, and N. W. Ashcroft, Phys. Rev. B **21**, 2248 (1980).

[36] M. Wojcik, M. Hauser, W. Li, S. Moon, and K. Xu, Nat. Commun. **6**, 7384 (2015).

[37] D. H. Huang, O. Roslyak, G. Gumbs, W. Pan, and A. A. Maradudin, Proc. SPIE **9961**, 996104 (2016).

[38] G. Gumbs and D. H. Huang, *Properties of Interacting Low-Dimensional Systems* (Wiley, Hoboken, NJ, 2011), Chap. 2.

[39] D. H. Huang, G. Gumbs, and O. Roslyak, Appl. Opt. **52**, 755 (2013).

[40] B. Wunsch, T. Stauber, F. Sols, and F. Guinea, New J. Phys. **8**, 318 (2006).

[41] P. Pyatkovskiy, J. Phys.: Condens. Matter **21**, 025506 (2008).

[42] O. Roslyak, G. Gumbs, and D. H. Huang, J. Appl. Phys. **109**, 113721 (2011).

[43] A. Principi, M. Polini, and G. Vignale, Phys. Rev. B **80**, 075418 (2009).

[44] T. Stauber and G. Gómez-Santos, Phys. Rev. B **82**, 155412 (2010).

[45] D. H. Huang and Y. Zhao, Phys. Rev. A **51**, 1617 (1995).

[46] A. F. Oskooi, D. Roundy, M. Ibanescu, P. Bermel, J. D. Joannopoulos, and S. G. Johnson, Comput. Phys. Commun. **181**, 687 (2010).